

Electronic Supplementary Information  
for

**Ultrafast excited state decay of natural UV filters: from intermolecular hydrogen bonds to conical intersection**

Peter S. Sherin,<sup>a,b,c,\*</sup> Yuri P. Tsentalovich,<sup>a,b</sup> Eric Vauthey,<sup>c</sup> Enrico Benassi<sup>b,d,\*</sup>

<sup>a</sup> *International Tomography Center SB RAS, Institutskaya street 3A, Novosibirsk, Russia*

<sup>b</sup> *Novosibirsk State University, Pirogova street 2, Novosibirsk, Russia*

<sup>c</sup> *Department of Physical Chemistry, University of Geneva, quai Ernest-Ansemet 30, Geneva, Switzerland*

<sup>d</sup> *School of Science and Technology, Nazarbayev University, Qabanbay Batyr Ave 53, Astana 010000, Kazakhstan*

**Corresponding Authors**

\* [petr.sherin@tomo.nsc.ru](mailto:petr.sherin@tomo.nsc.ru), [enrico.benassi@nu.edu.kz](mailto:enrico.benassi@nu.edu.kz)

<b>Table of content</b>	<b>page number</b>
Experimental data	2-5
<i>Fig. S1, Fig. S2</i>	2
<i>Fig. S3</i>	3
<i>Fig. S4</i>	4
<i>Fig. S5</i>	5
Calculation data	6-17
<i>Fig. S6</i>	6
<i>Fig. S7</i>	7
<i>Tables S1 and S2, Scheme S1</i>	8
<i>Fig. S8, Table S3</i>	9
<i>Table S4</i>	10
<i>Fig. S9A</i>	11
<i>Fig. S9B</i>	12
<i>Fig. S10, Table S5</i>	13
<i>Fig. S11</i>	14-15
<i>Critical point analysis</i>	16
<i>Fig. S12</i>	17-18
Experimental and Calculation Section	19-25
<i>Materials and experimental setups</i>	19-20
<i>Calculation details</i>	20-25
References	25-27

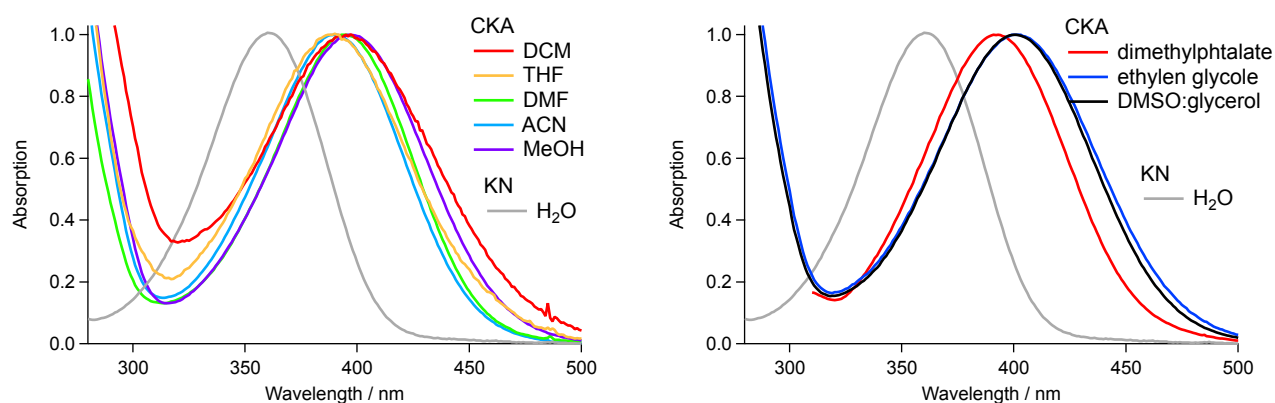


Fig. S1. Experimental absorption spectra of CKA in various organic solvents. Absorption spectrum of KN in aqueous solution is shown as grey curve is for reference. Solvent abbreviations: DCM = dichloromethane, THF = tetrahydrofurane, DMF = dimethyl formamide; ACN = acetonitrile; MeOH = methanol.

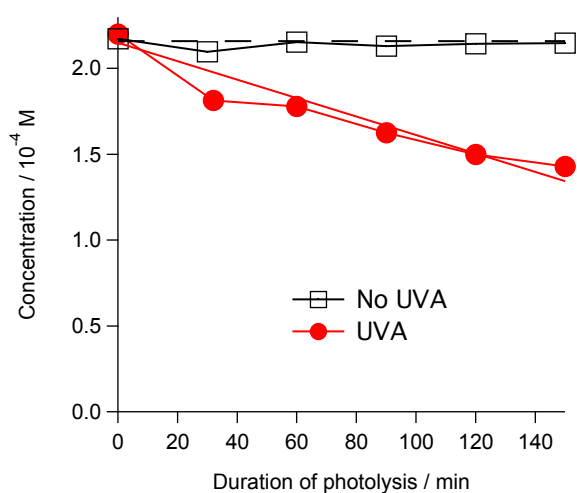


Fig. S2. Concentration profiles of CKA during the anaerobic photolysis (red circles) and control experiment without UVA light (black open squares) obtained by HPLC analysis of aliquots from irradiated samples. Solid red line: best fit in linear approximation. Standard error is 5%. Data are corrected for the absorption at 258 nm of 0.5 mM phenylalanine used as internal standard.

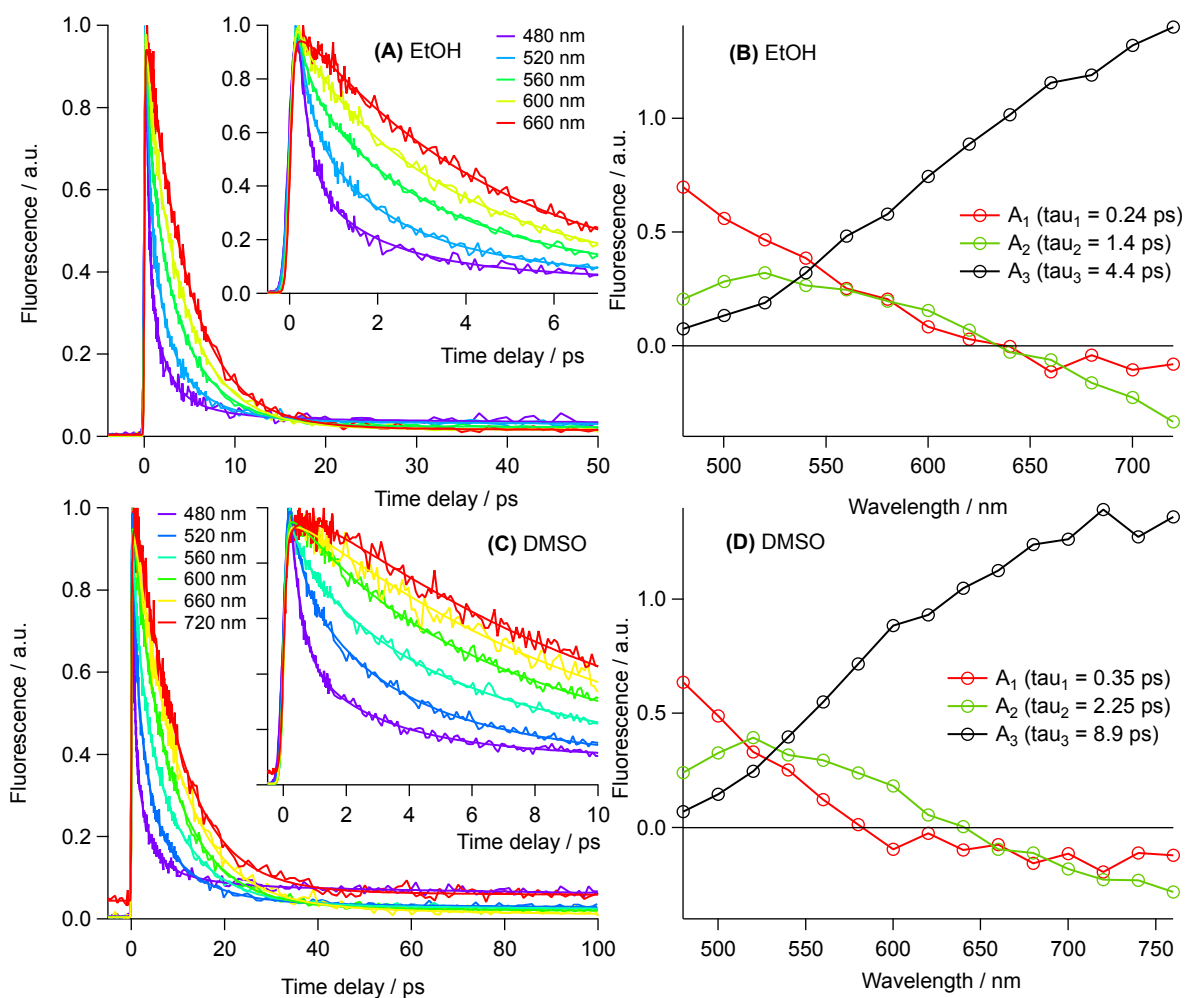


Fig. S3. (A, C): Fluorescence time profiles recorded with CKA in EtOH and DMSO, respectively, after 430 nm excitation; smooth lines: the best fits. Insets: the early dynamics for the same data. (B, D): Normalized amplitudes obtained in the global analysis of the fluorescence data in (A, C).

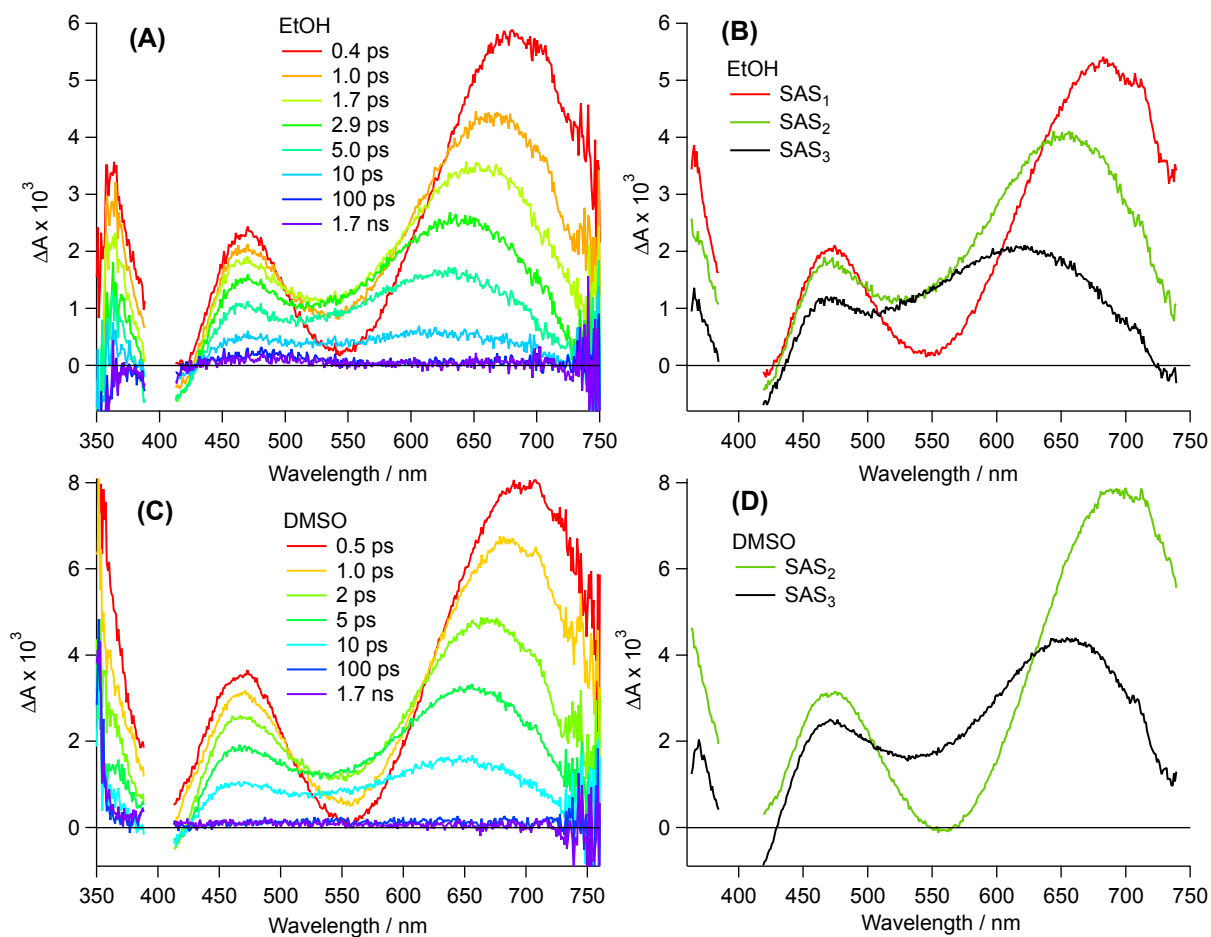


Fig. S4. (A, C): TA spectra recorded with CKA in EtOH and DMSO, respectively, after 400 nm excitation. (B, D):  $SAS_i(\lambda)$ ,  $i = 1,2,3$  obtained in the global analysis of TA data in (A, C).

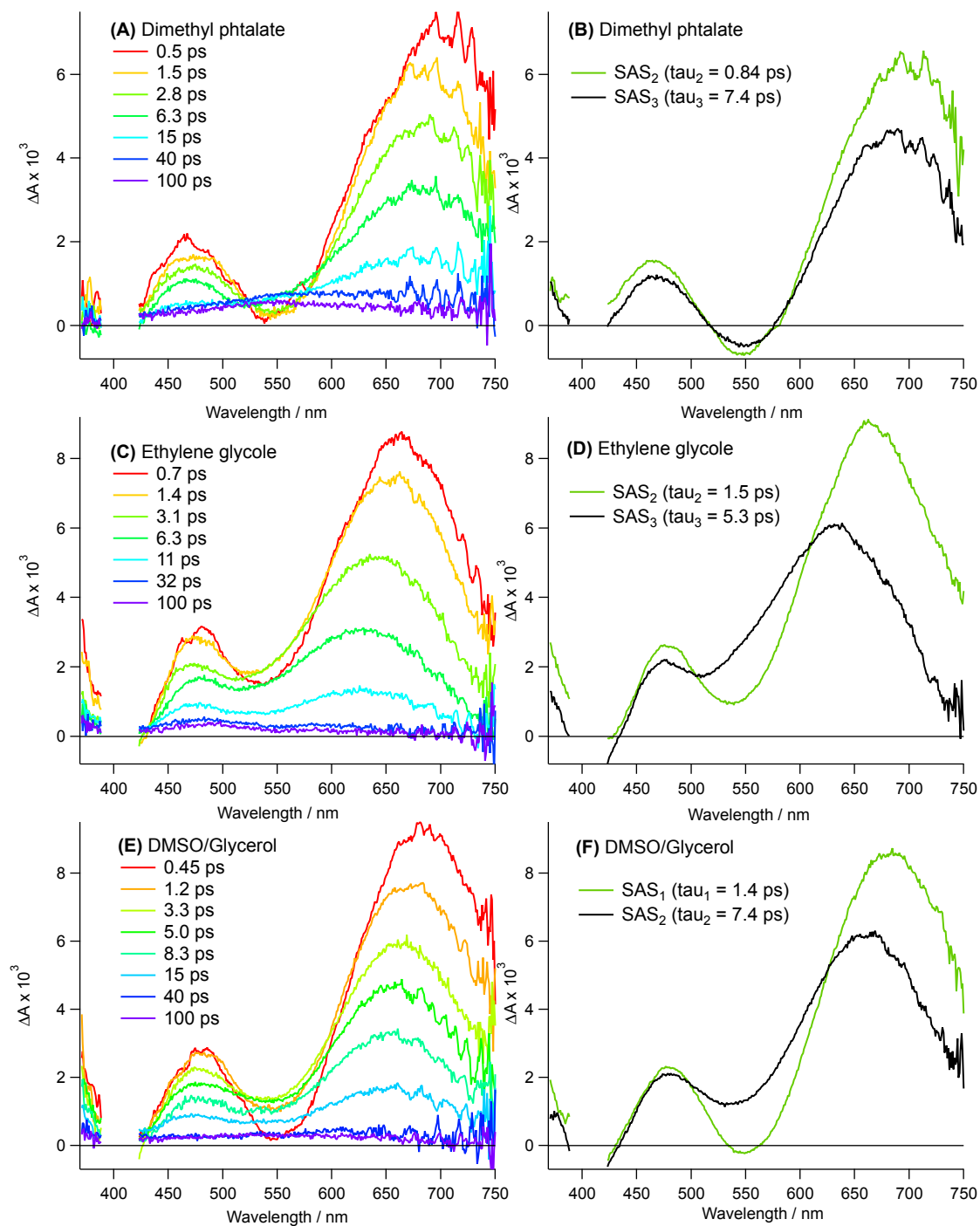


Fig. S5. (A, C, E): TA spectra recorded with CKA in dimethyl phthalate, ethylene glycol and DMSO/Glycerol (5/6 w/w), respectively, after 400 nm excitation. (B, D, F):  $SAS_i(\lambda)$ ,  $i = 1, 2$  obtained in the global analysis of TA data in (A, C, E).

## Ground State Optimised Geometries

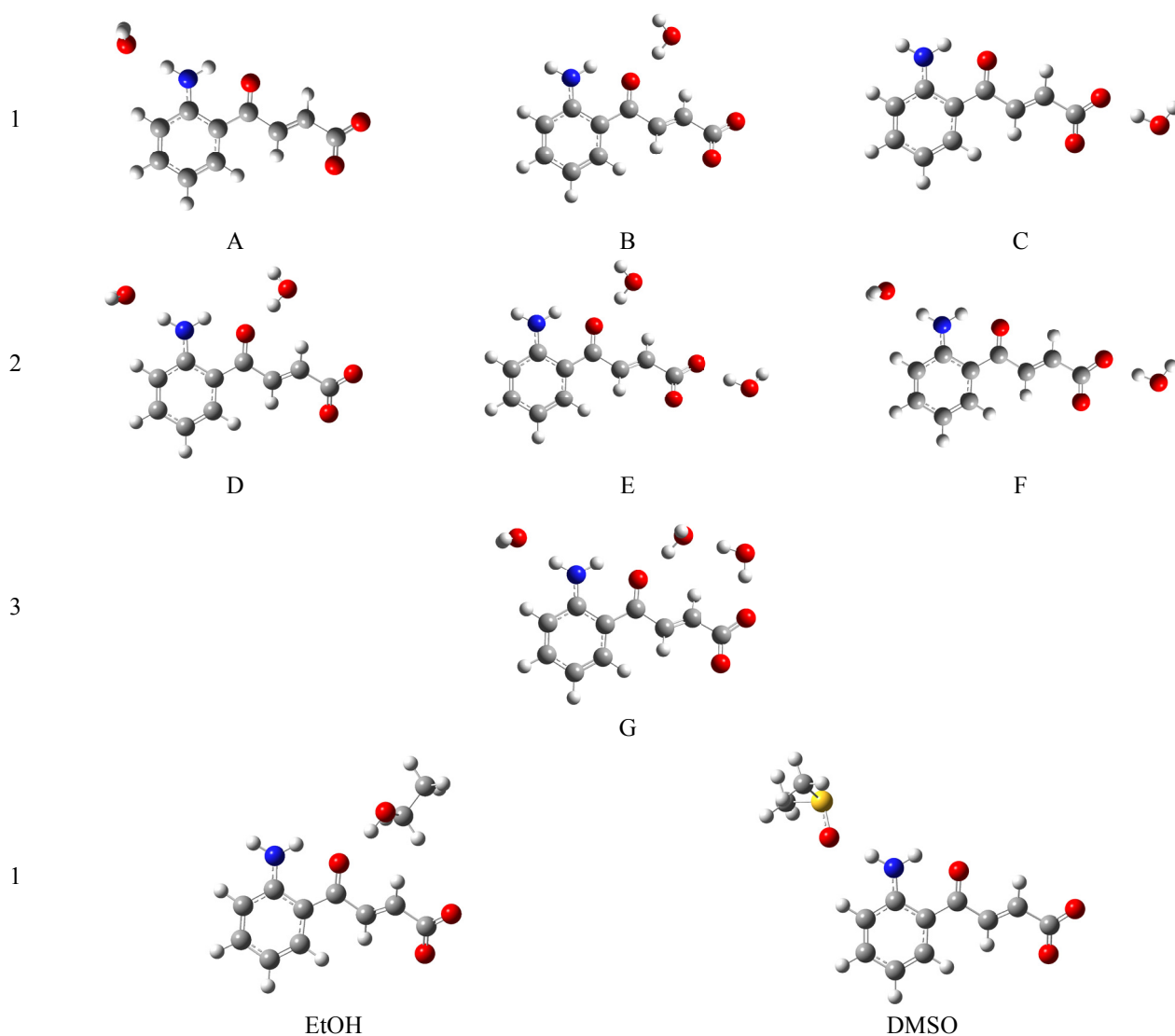


Fig. S6. DFT optimized ground state ( $S_0$ ) geometries of *trans* CKA<sup>-</sup> in H<sub>2</sub>O, EtOH and DMSO. Solvents effects were introduced within a Mixed Micro-Explicit / Implicit Solvation (IEF-PCM model). For aqueous solution different numbers of explicit solvent molecules were used (A-C: 1 explicit H<sub>2</sub>O molecule; D-F: 2 explicit H<sub>2</sub>O molecules, G: 3 explicit H<sub>2</sub>O molecules). The energies of *trans* CKA<sup>-</sup> for A-G configurations of micro-solvation are given below. Legend of colours: white (hydrogen), grey (carbon), blue (nitrogen), red (oxygen), yellow (sulphur).

	$n$ molecules of H <sub>2</sub> O	$\Delta E^*$ / eV
A	1	0.547
B	1	0.607
C	1	0.415
D	2	0.426
E	2	0.239
F	2	0.297
G	3	0.000

$$\Delta E \equiv [E(I) - n E(\text{H}_2\text{O})] - E_{(\text{min})} \quad (I = \text{A, B, } \dots \text{ G}).$$

## Excited State $S_1$ Optimised Geometries

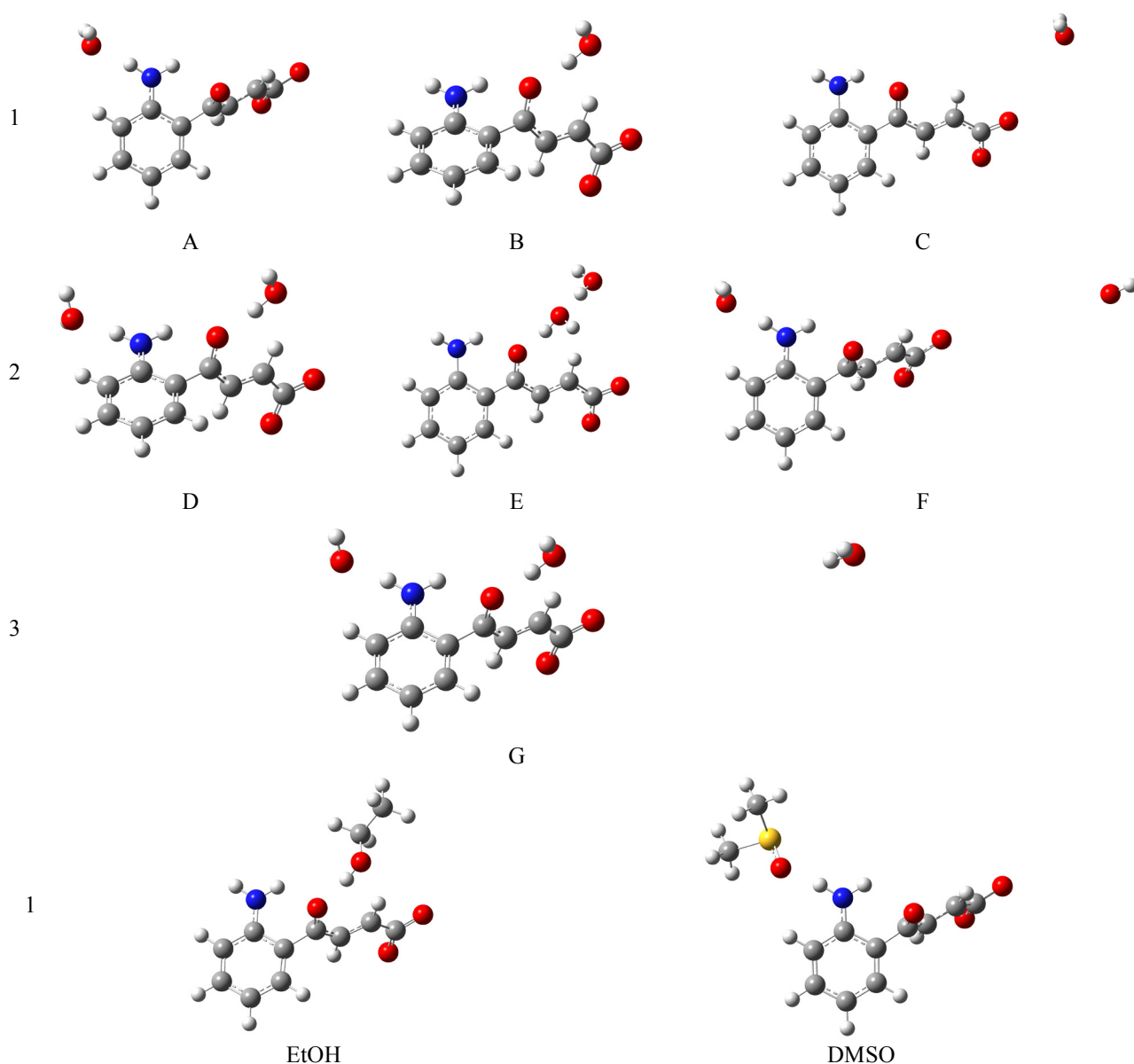


Fig. S7. TD-DFT optimized excited state ( $S_{1r}$ ) geometries of *trans* CKA<sup>-</sup> in H<sub>2</sub>O, EtOH and DMSO. Solvents effects were introduced within a Mixed Micro-Explicit / Implicit Solvation (IEF-PCM model). For aqueous solution different number of explicit solvent molecules were used (A-C: 1 explicit H<sub>2</sub>O molecule; D-F: 2 explicit H<sub>2</sub>O molecules, G: 3 explicit H<sub>2</sub>O molecules). The energies of *trans* CKA<sup>-</sup> for A-G configurations of micro-solvation are given below. Legend of colours: white (hydrogen), grey (carbon), blue (nitrogen), red (oxygen), and yellow (sulphur).

	$n$ molecules of H <sub>2</sub> O	$\Delta E^*$ / eV
A	1	0.350
B	1	0.405
C	1	0.496
D	2	0.117
E	2	0.000
F	2	0.504
G	3	0.118

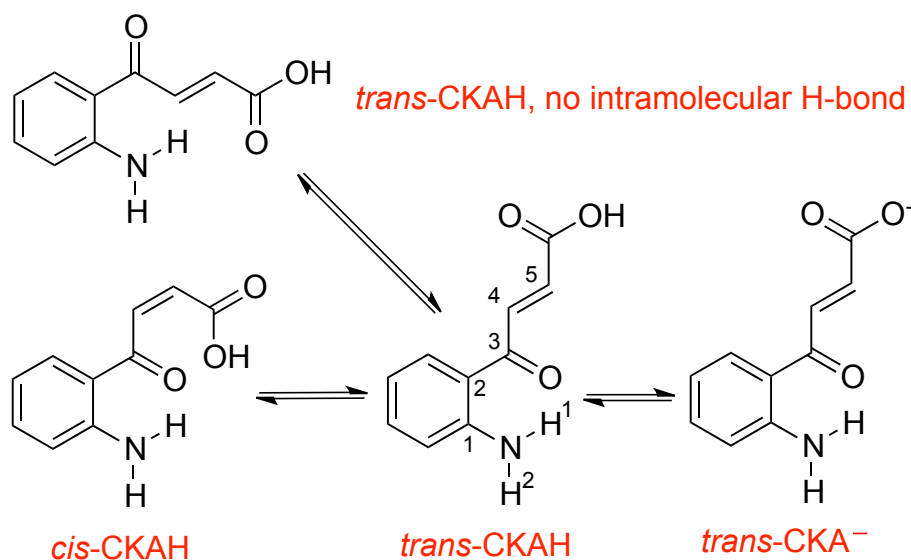
\*  $\Delta E \equiv [E(I) - n E(\text{H}_2\text{O})] - E_{(\text{min})}$  (I = A, B, ... G).

Table S1. Solvation reaction energies,  $\Delta E^{(P-R)} = E^{(P)} - E^{(R)}$ . Legend: P = products; R = reactants; S = solvent molecule. Level of theory: DFT B3LYP[GD3BJ]/6-311+G\*\*//IEF-PCM(SMD).

$\Delta E^{(P-R)} / (\text{eV})$	CKAH + S = CKA <sup>-</sup> + SH <sup>+</sup>	
	<i>trans</i>	<i>cis</i>
H <sub>2</sub> O	-1.583	-1.889
EtOH	-1.013	-1.226
DMSO	-0.529	-0.838

Table S2. Isomerization electronic energies,  $\Delta E^{(\text{cis-trans})} = E^{(\text{cis})} - E^{(\text{trans})}$ . Level of theory: DFT B3LYP[GD3BJ]/6-311+G\*\*//IEF-PCM(SMD).

$\Delta E^{(\text{cis-trans})} / (\text{eV})$	CKAH	CKA <sup>-</sup>
vacuum	2.683	1.992
H <sub>2</sub> O	2.406	1.837
EtOH	1.217	1.743
DMSO	2.405	1.881



Scheme S1. Chemical structures of various form of CKA (duplication of Scheme 1 in the main text for the Reader convenience).



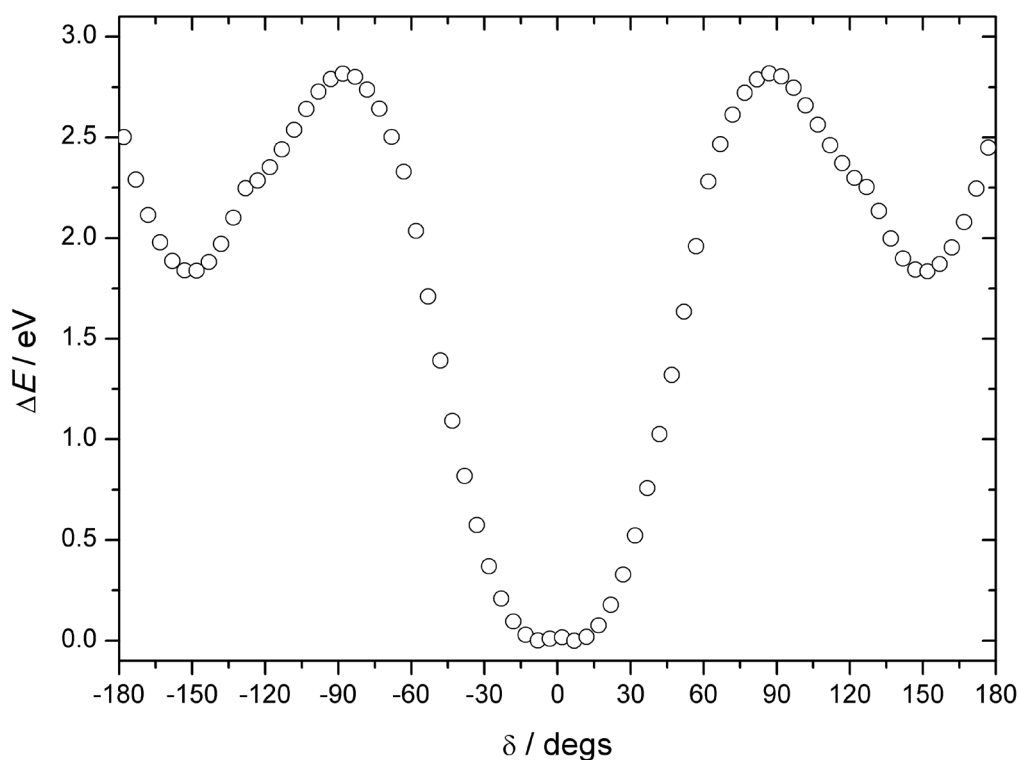
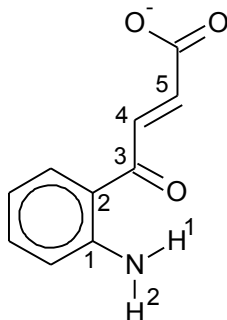


Fig. S8. Scan of the PES around  $\delta(C^{(1)}C^{(2)}C^{(3)}O)$  of *trans*-CKA<sup>-</sup> in aqueous solution (IEF-PCM) at room temperature. For atom numeration, see chemical structure of CKA presented in Scheme S1 (Scheme 1 of the main text).

Table S3. Electronic energy of ground state ( $S_0$ ), Frank-Condon ( $S_{1v}$ ) and “relaxed” ( $S_{1r}$ ) first singlet excited states. Level of theory: (TD-)DFT B3LYP[GD3BJ]/6-311+G\*\*//IEF-PCM(UFF).

PCM	DMSO	EtOH	H <sub>2</sub> O
$E(S_0)$ / a.u.	-666.496780797	-666.494468700	-666.497841815
$E(S_{1v})$ / a.u.	-666.386621166	-666.383659988	-666.387983784
$E(S_{1r})$ / a.u.	-666.406481038	-666.403418496	-666.407887018
$\Delta E(S_{1v}-S_0)$ / eV	2.998	3.015	2.989
$\Delta E(S_{1v}-S_{1r})$ / eV	0.540	0.538	0.542
expl. / PCM	DMSO	EtOH	H <sub>2</sub> O
$E(S_0)$ / a.u.	-1219.71641952	-821.552851877	-742.936228161
$E(S_{1v})$ / a.u.	-1219.60745749	-821.443344788	-742.827631099
$E(S_{1r})$ / a.u.	-1219.63055192	-821.465489561	-742.850164515
$\Delta E(S_{1v}-S_0)$ / eV	2.965	2.980	2.955
$\Delta E(S_{1v}-S_{1r})$ / eV	0.628	0.603	0.613

Table S4. Some of geometric parameters of ground ( $S_0$ ) and “relaxed” first singlet excited ( $S_{1r}$ ) electronic states of *trans*-CKA<sup>-</sup> in DMSO, EtOH, and H<sub>2</sub>O calculated. Solvent effects are included within the PCM (top) or combining the PCM with a few explicit solvent molecules (bottom): one for DMSO and EtOH and two for H<sub>2</sub>O. Distances are in Å, dihedral angles in degrees. The structure of CKA with atom numeration is shown below for convenience. Level of theory: (TD-)DFT B3LYP[GD3BJ]/6-311+G\*\*//IEF-PCM(UFF).



QM (PCM)	DMSO		EtOH		H <sub>2</sub> O	
	$S_0$	$S_{1r}$	$S_0$	$S_{1r}$	$S_0$	$S_{1r}$
C <sup>(2)</sup> C <sup>(3)</sup>	1.477	1.515	1.478	1.516	1.477	1.515
C <sup>(3)</sup> C <sup>(4)</sup>	1.490	1.412	1.490	1.412	1.490	1.412
C <sup>(4)</sup> C <sup>(5)</sup>	1.344	1.390	1.344	1.390	1.344	1.390
C <sup>(3)</sup> O	1.249	1.289	1.249	1.290	1.250	1.289
NH <sup>(1)</sup>	1.014	1.019	1.014	1.019	1.014	1.018
OH <sup>(1)</sup>	1.898	2.169	1.896	2.152	1.900	2.177
NH <sup>(1)</sup> /OH <sup>(1)</sup>	0.534	0.470	0.535	0.474	0.534	0.468
C <sup>(1)</sup> C <sup>(2)</sup> C <sup>(3)</sup> C <sup>(4)</sup>	172.7	117.6	172.6	117.9	172.6	117.5
C <sup>(1)</sup> C <sup>(2)</sup> C <sup>(3)</sup> O	6.9	61.9	7.0	61.5	6.9	62.0
C <sup>(5)</sup> C <sup>(4)</sup> C <sup>(3)</sup> O	13.8	3.0	13.7	2.9	13.9	2.9
QM (1 expl.)	DMSO		EtOH		H <sub>2</sub> O	
	$S_0$	$S_{1r}$	$S_0$	$S_{1r}$	$S_0$	$S_{1r}$
C <sup>(2)</sup> C <sup>(3)</sup>	1.473	1.513	1.471	1.512	1.469	1.510
C <sup>(3)</sup> C <sup>(4)</sup>	1.491	1.412	1.486	1.408	1.486	1.409
C <sup>(4)</sup> C <sup>(5)</sup>	1.344	1.392	1.344	1.390	1.344	1.390
C <sup>(3)</sup> O	1.251	1.289	1.255	1.297	1.256	1.297
NH <sup>(1)</sup>	1.013	1.015	1.013	1.016	1.013	1.015
OH <sup>(1)</sup>	1.898	2.433	1.908	2.358	1.910	2.437
NH <sup>(1)</sup> /OH <sup>(1)</sup>	0.534	0.417	0.531	0.431	0.530	0.416
O...H*	1.914	1.737	1.852	1.745	1.833	1.733
C <sup>(1)</sup> C <sup>(2)</sup> C <sup>(3)</sup> C <sup>(4)</sup>	174.0	108.9	172.5	109.8	172.8	107.3
C <sup>(1)</sup> C <sup>(2)</sup> C <sup>(3)</sup> O	5.5	70.6	7.2	69.2	6.8	71.4
C <sup>(5)</sup> C <sup>(4)</sup> C <sup>(3)</sup> O	13.9	2.0	22.5	2.8	22.8	1.7

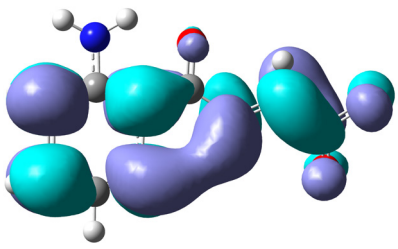
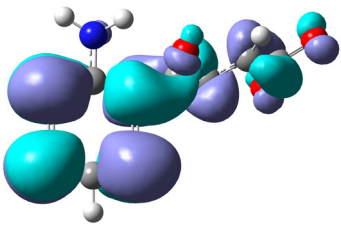
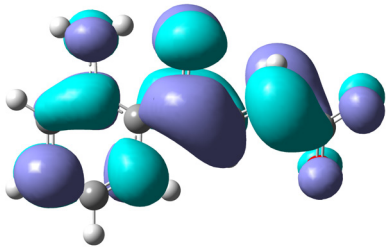
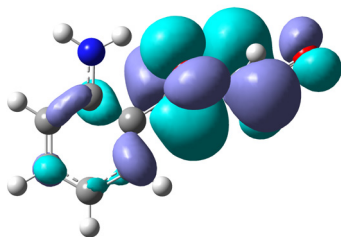
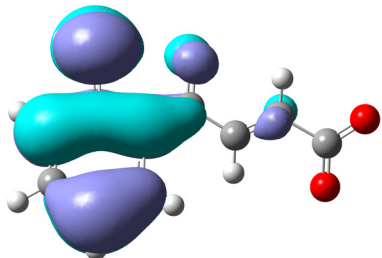
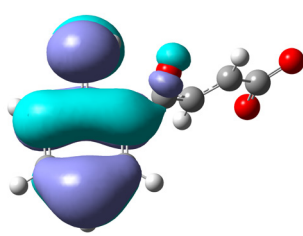
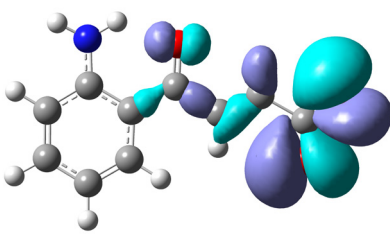
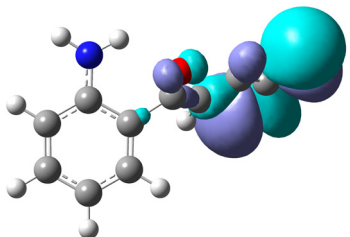
PCM	$S_0$	$S_{1r}$
LUMO + 1		
LUMO		
HOMO		
HOMO - 1		

Fig. S9A. Distribution of electron density for frontier molecular orbitals (HOMO-1, HOMO, LUMO and LUMO+1) in ground ( $S_0$ ) and “relaxed” first singlet excited ( $S_{1r}$ ) electronic states of *trans*-CKA<sup>-</sup> in aqueous solution. Level of theory: (TD-)DFT B3LYP[GD3BJ]/6-311+G\*\*//IEF-PCM(UFF).

expl.	$S_0$	$S_{1r}$
LUMO + 1		
LUMO		
HOMO		
HOMO - 1		

Fig. S9B. Distribution of electron density for frontier molecular orbitals (HOMO-1, HOMO, LUMO and LUMO+1) in ground ( $S_0$ ) and “relaxed” first singlet excited ( $S_{1r}$ ) electronic states of *trans*-CKA<sup>-</sup> in aqueous solution (explicit micro-solvation plus continuum model). Level of theory: (TD-)DFT B3LYP[GD3BJ]/6-311+G\*\*//IEF-PCM(UFF).

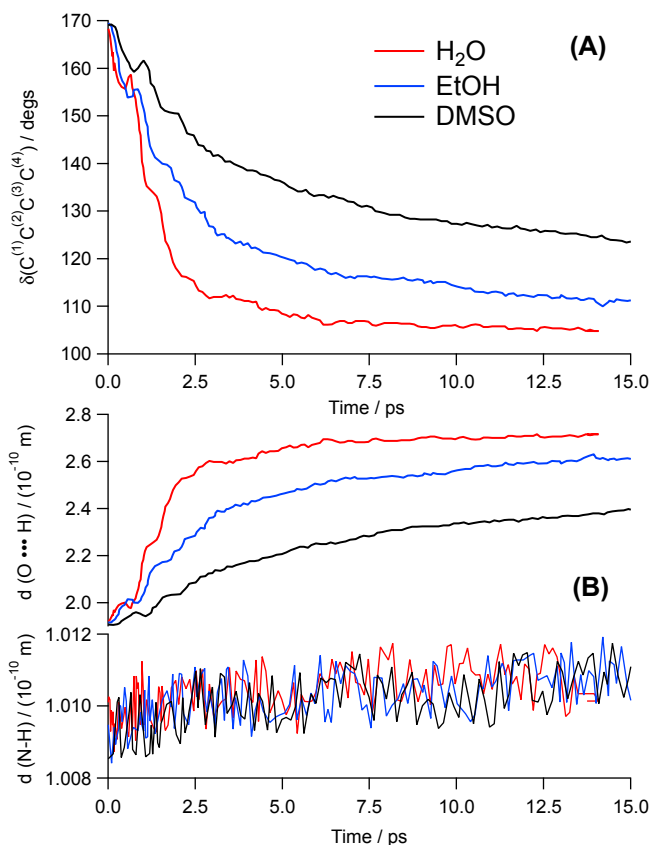


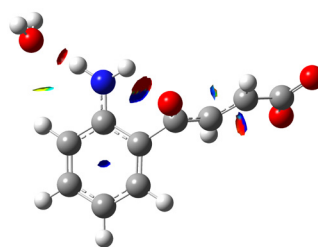
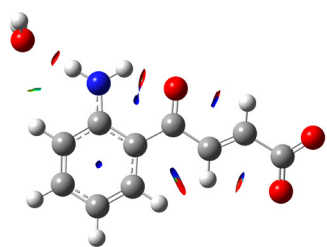
Fig. S10. Time profiles of (A) average dihedral angle  $\delta(C^{(1)}C^{(2)}C^{(3)}C^{(4)})$ , (B) average distances N-H<sup>(1)</sup> and O•••H<sup>(1)</sup> of *trans*-CKA<sup>-</sup> solution (DMSO, EtOH and H<sub>2</sub>O) along the QM/MM simulations.

Table S5. Electronic energy of ground state (S<sub>0</sub>) and Frank-Condon first (S<sub>1v</sub>) and second (S<sub>2v</sub>) singlet excited states of *trans*-CKA<sup>-</sup> in DMSO and H<sub>2</sub>O solutions depending on the H atom position between amino and carbonyl groups.

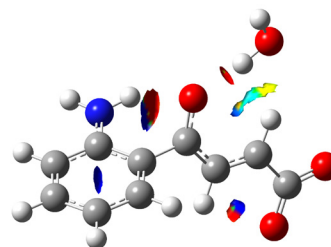
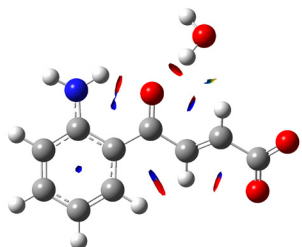
Level of theory: (TD-)DFT B3LYP[GD3BJ]/6-311+G\*\*//IEF-PCM(UFF).

<b>DMSO</b>			
	S <sub>0</sub>	S <sub>1v</sub>	S <sub>2v</sub>
-NH <sub>2</sub> •••O=	0.000	2.983	3.150
-NH•••H•••O-	5.033	5.919	6.321
-NH•••HO-	1.744	4.211	4.480
<b>H<sub>2</sub>O</b>			
	S <sub>0</sub>	S <sub>1v</sub>	S <sub>2v</sub>
-NH <sub>2</sub> •••O=	0.000	2.354	3.158
-NH•••H•••O-	5.028	5.392	6.446
-NH•••HO-	1.743	3.579	4.515

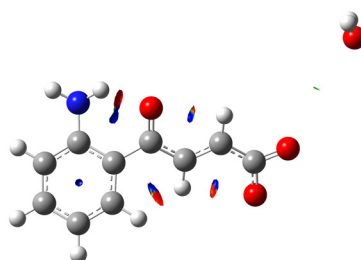
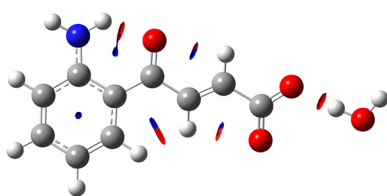
H<sub>2</sub>O A



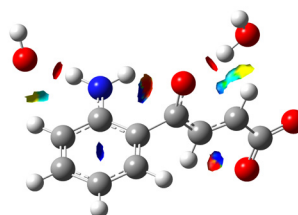
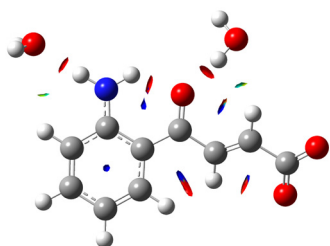
B



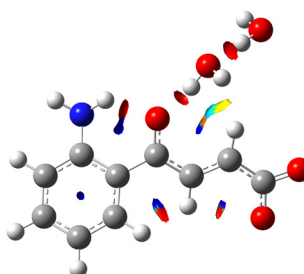
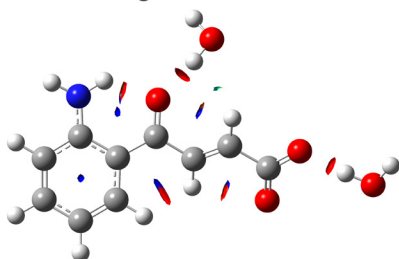
C



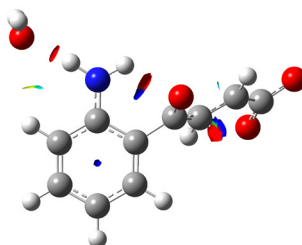
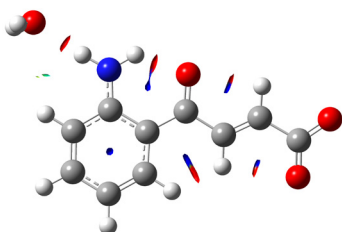
D



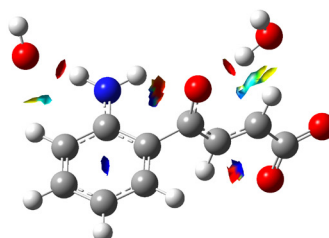
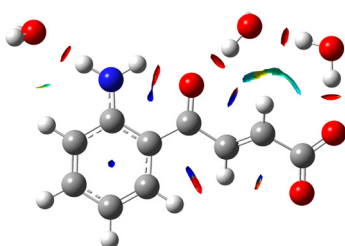
E



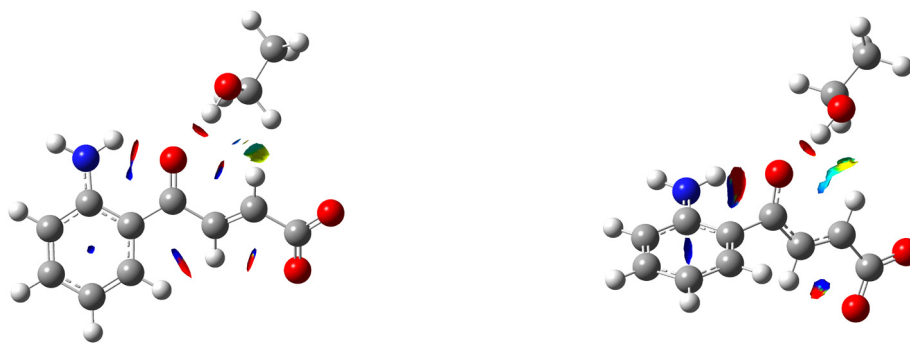
F



G



EtOH



DMS  
O

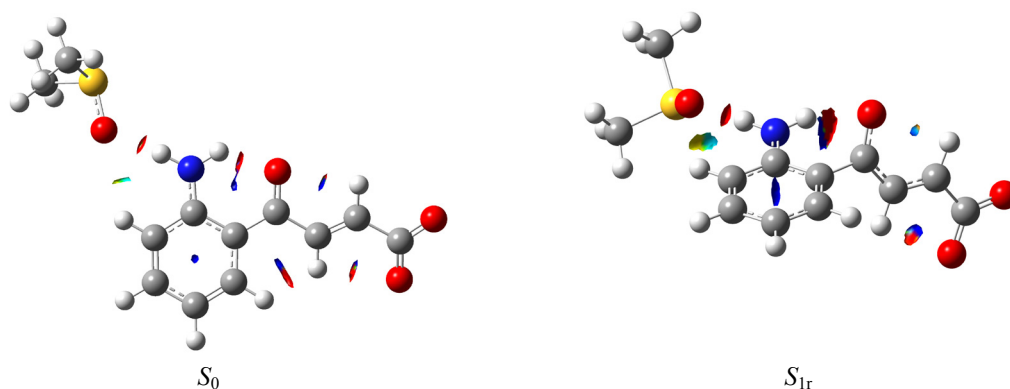


Fig. S11. Plots of the NCI isosurfaces ( $s = 0.5$  a.u. and a blue-green-red colour scale from  $-0.01$  a.u.  $< \text{sign}(\lambda_2) \rho(r) < +0.01$  a.u.) of  $S_0$  and relaxed  $S_1$  states of CKA in different solvents. Legend of colours for the NCI isosurfaces: red (strongly attractive), yellow-green (weakly attractive), green-turquoise (weakly repulsive), and blue (strongly repulsive).

*Topological AIM Analysis. Search of critical points (see Figure S12).*

This analysis was done additionally to RGD calculations (Figure S11).

Within his AIM theory, Bader describes four different types of critical points (CPs):

- **(3, -3)** CP: The electron density falls down in all three perpendicular directions of space. This is a local maximum of electron density.
- **(3, -1)** CP: The electron density falls down in two perpendicular directions of space and rises in the third direction. This is a saddle point of electron density with a maximum of electron density in two directions of space and a minimum in the third one.
- **(3, +1)** CP: The electron density falls in one direction of space and rises in the two other perpendicular directions of space. Again this is a saddle point with a maximum in one and a minimum in two directions of space.
- **(3, +3)** CP: This is a local minimum with electron density rising in all three directions of space.

The chemical meaning is:

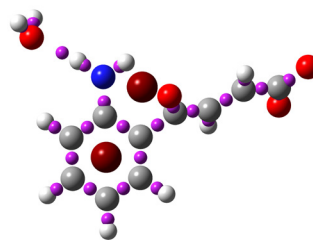
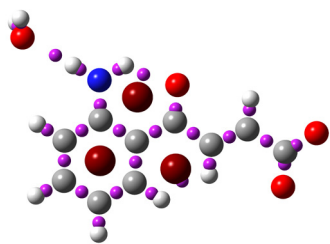
- **(3, -3)** CP: This is the position of an atom. For all atoms except hydrogen it is also the position of the nuclei. The point therefore is also called an *atomic critical point* (ACP).
- **(3, -1)** CP: These points are between two neighbouring atoms defining a bond between them. This point is therefore also called a *bond critical point* (BCP). These are depicted in pink in figure.
- **(3, +1)** CP: This point is to be found in the middle of several bonds forming a ring. It is also called a *ring critical point* (RCP). These are depicted in wine red in figure.
- **(3, +3)** CP: This point is found when several rings form a cage and is therefore called a *cage critical point* (CCP).

BCPs and RCPs are those of higher interest in our investigation, since they show formation of bond or the increase of structural rigidity upon photoexcitation.

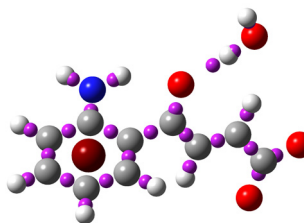
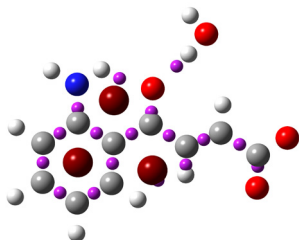


Critical points

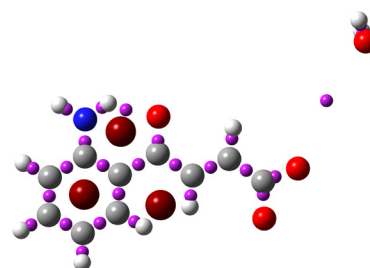
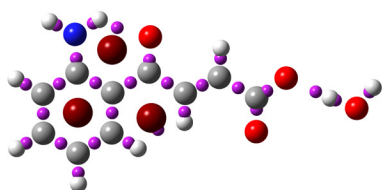
H<sub>2</sub> A  
O



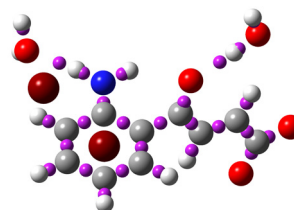
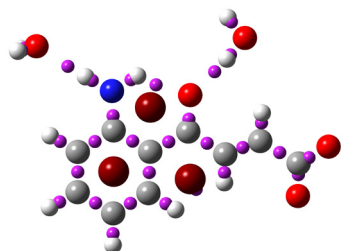
B



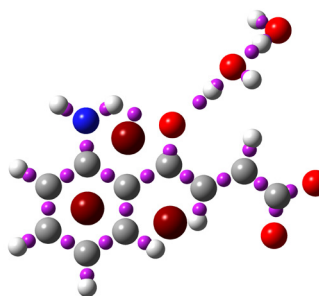
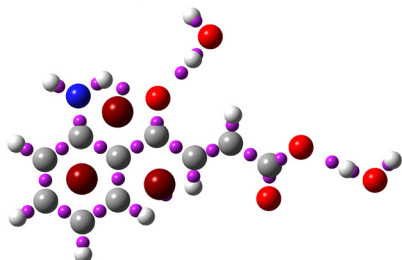
C



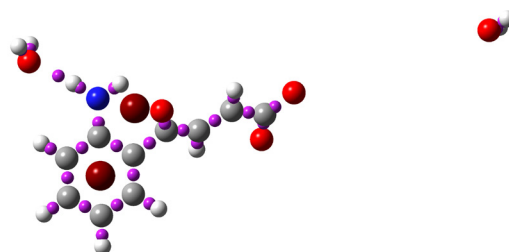
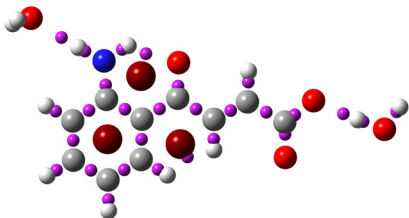
D



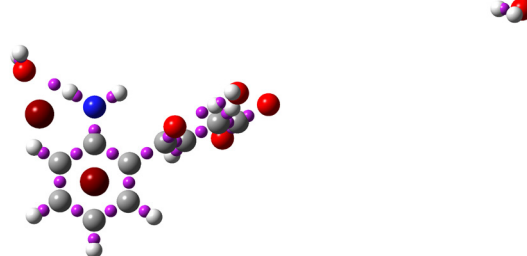
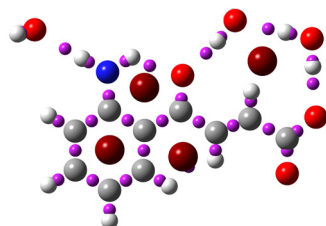
E



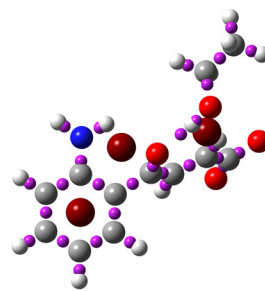
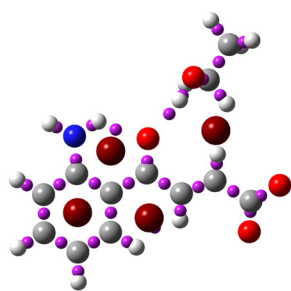
F



G



EtOH



DMSO

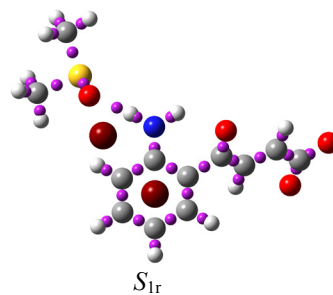
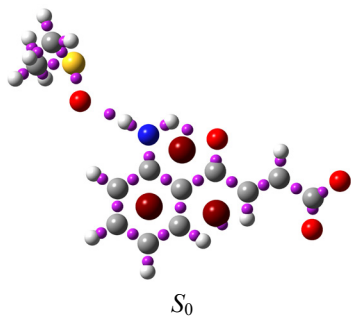


Fig. S12. Topological Analysis of  $S_0$  and relaxed  $S_1$  of CKA in different solvents. Bond Critical Points are depicted in pink and Ring Critical Points are depicted in wine red.

## Experimental and Calculation section

### *Materials*

D,L-kynurenine (KN) was from Sigma/Aldrich and used as received. Organic solvents, dimethyl sulfoxide (DMSO), dimethyl formamide (DMF), acetonitrile (ACN), ethanol (EtOH), methanol (MeOH), dimethyl phthalate, ethylene glycol, glycerol of highest purity from Sigma/Aldrich or Fluka and deuterated water from Armar were used as received. H<sub>2</sub>O was distilled and deionized (18 MΩ).

### *Synthesis and purification*

Deaminated kynurenine, 4-(2-aminophenyl)-4-oxocrotonic acid (CKA), was obtained via the incubation of KN (7 mM, pH 9) at 70°C during 24 hours. After incubation and filtration, the solution was separated by High Performance Liquid Chromatography (HPLC) system (LC 1200, Agilent, USA) equipped with a multiple wavelength UV-Vis detector on a C16 preparative column (16×250 mm, 7 μm, Diasorb-130-C16-T; BioChimMac ST, Russia). Separations were performed with mobile phases A (0.05% of trifluoroacetic acid in water) and B (ACN) using the gradient: 0% B (0–3 min), 0–30% B (3–5 min), 30–55% B (5–35 min), 55–100% B (35–37 min). The flow rate was 4 mL/min, the injection volume was 1 mL, and the detection was performed simultaneously at five wavelengths – 280, 320, 360, 380 and 400 nm. The fractions containing CKA (retention time 28.7 min) were collected and separated in two parts and both parts were separately dried via rotational vaporization. Then, one part was dissolved in 500 μl of MeOH and the second part in 500 μl of DMF; both samples were stored at –20°C. CKA was stored in organic solvents in order to prevent the oxidation in the solid state. The subsequent HPLC analysis showed the purity of CKA as 98%. The identity of CKA was verified by mass-spectrometry using an Esquire6000 (Bruker Daltonics, Germany). The samples for time-resolved experiments were prepared by dissolution of 20 μl of stock CKA solutions in MeOH/DMF in 800 μl of pure protic/aprotic solvents, respectively.

### *Steady-state optical measurements*

UV-visible electronic absorption spectra were recorded with an Agilent HP 8453 (Agilent, USA) or a Cary 50 (Varian, USA) spectrophotometers.

### *Steady-state photolysis*

Samples containing PBS solution of 0.25 mM CKA and 0.5 mM phenylalanine in 10 × 8 mm<sup>2</sup> quartz cell (sample volume 2.5 ml) were irradiated with a DRSh-1000 mercury lamp from Stella Ltd (Moscow, Russia). Phenylalanine was added as internal standard, which does not absorb at wavelengths shorter than 280 nm. A water filter was used to cut off infrared light, and the 340–430 nm region was selected with a set of UV glass filters. Actinometry was performed using an aqueous solution of potassium ferri-oxalate according to standard methods.<sup>1</sup> The intensity of light on the sample in the 340–430 nm region was equal to  $(1.1 \pm 0.1) \times 10^{18}$  quanta per second. The solutions were bubbled with argon for 15 min prior to and during irradiation. During photolysis, samples (100 μL) were periodically taken off with a syringe, diluted with water up to 200 μL and stored at 4 °C until analysed by HPLC. A control experiment was performed under the same conditions without irradiation. The HPLC analysis of the irradiated samples was performed on a 4.6 × 150 mm, 5 μm, ZORBAX Eclipse XBD-C18 analytical column with the gradient used for CKA isolation. The flow rate was 0.5 mL/min, the 50 μL of sample was injected with the use of autosampler thermostated at 4 °C. The chromatograms were recorded at 280, 320, 360 and 400 nm and the peak areas integrated using Agilent ChemStation software.

### ***Time-resolved fluorescence measurements***

The fluorescence dynamics was recorded using a fluorescence up-conversion setup described in details elsewhere.<sup>2,3</sup> Briefly, a part of the output of a tunable mode-locked Ti:sapphire laser (Spectra Physics “MaiTai”) was frequency-doubled and used to excite the sample at 400 nm. The polarization of the probe pulses was at the magic angle relative to that of the gate pulses at 800 nm. The fluorescence was gated by sum-frequency mixing with the fundamental of the oscillator output. The up-converted UV photons were directed into a monochromator and detected by a photomultiplier tube with photon counting electronics. The sample solutions were kept in a 1.0 mm thick spinning cell and had an absorbance of about 0.2 at the excitation wavelength. The full width at half-maximum (FWHM) of the instrument response function was around 210 fs.

### ***Transient absorption (TA) measurements***

The TA dynamics at femtosecond time scale was carried out with the experimental setup described in refs.<sup>4,5</sup> Excitation was performed at 400 nm using the frequency doubled output of a standard 1 kHz amplified Ti:Sapphire system (Spectra-Physics). The pump intensity on the sample was around 1.5 mJ/cm<sup>2</sup>. Probing was achieved with a white-light continuum obtained by focusing a small fraction of the 800 nm pulses in a CaF<sub>2</sub> plane window. The polarization of the probe pulses was at the magic angle relative to that of the pump pulses. All spectra were corrected for the chirp of the white light probe pulses. The FWHM of the instrument response function was ca. 200 fs. The sample solutions were placed in a 1 mm thick quartz cell where they were continuously stirred by N<sub>2</sub>-bubbling. Their absorbance at the excitation wavelength was around 0.2.

TA dynamics at nanosecond scale was recorded with Laser Flash Photolysis (LFP) setup described earlier.<sup>6,7</sup> Briefly, samples in a quartz cell (inner dimensions 10 mm × 8 mm) were irradiated with a Quanta-Ray LAB-130-10 Nd:YAG laser (355 nm, pulse duration 8 ns, pulse energy up to 135 mJ). The dimensions of the laser beam at the front of the cell were 2.5 mm × 8 mm. The probe system includes a DKSh-150 xenon short-arc lamp connected to a high current pulser, a Newport 78025 monochromator, a 9794B photomultiplier (Electron Tubes Ltd.), and a LeCroy WaveRunner 104MXi digital oscilloscope. The probe light, concentrated in a rectangular of 2.5 mm height and 1 mm width, passed through the cell along the front (laser irradiated) window. Thus, in all experiments the excitation optical length was 1 mm, and the probe optical length was 8 mm. All solutions were bubbled with argon or oxygen for 15 minutes prior to and during irradiation.

### ***Computational Details***

#### ***Ground state***

The molecular system computationally investigated was the protonated (neutral) and deprotonated (anionic) form of *trans* and *cis* CKA. In the case of *trans* CKA<sup>-</sup> (Scheme S1), four different rotamers were considered, *viz.*, wherein the dihedral angles  $\delta(C^{(1)}C^{(2)}C^{(3)}C^{(4)})$  and  $\delta(C^{(2)}C^{(3)}C^{(4)}C^{(5)})$  were set in *s-trans* and *s-cis* conformation. The ground state geometries of the conformers of neutral CKAH and anionic CKA<sup>-</sup> were fully optimized in gas phase at Density Functional Theory (DFT) level. Three different functionals were used (*viz.*, B3LYP,<sup>8</sup> M06-2X,<sup>9</sup> and  $\omega$ -B97-X<sup>10</sup>) coupled with two different Pople’s basis sets (*viz.*, 6-311+G\*\*<sup>11</sup> and 6-311++G\*\*<sup>12,13</sup>). The D3 version of Grimme’s semi-empirical dispersion with Becke-Johnson damping GD3BJ<sup>14</sup> was included in case of B3LYP and  $\omega$ -B97-X functionals.

Presence of imaginary frequencies was checked in harmonic approximation and minima were found to be “genuine.” Thermochemical quantities were also computed in harmonic approximation at  $T = 298.15$  K and  $p = 1.0$  atm.

The ground state geometries of different conformers of CKAH and CKA<sup>-</sup> were fully optimized also in solvated phase (*vide infra*) at DFT B3LYP[GD3BJ]/6-311+G\*\* level. Harmonic frequencies and thermochemical quantities were also computed as for the gas phase; no imaginary frequencies were found. Solvents and their protonated (cationic) forms were also fully optimized in solvated phase at the same level of theory, with calculation of harmonic frequencies and thermochemical quantities.

After this preliminary exploration, *trans*-CKAH (in gas phase) and *trans*-CKA<sup>-</sup> (in solvated phase) in the conformation forming intra-molecular hydrogen bond (IHB), as depicted in Scheme S1, were found to be largely the most stable. Subsequent calculations refer to this rotamer only.

The potential energy surface (PES) was explored *via* a relaxed scanning around the  $\delta(\text{C}^{(1)}\text{C}^{(2)}\text{C}^{(3)}\text{O})$  dihedral angle, both in gas and solvated phase, from -180 degs to 180 degs with 5-deg steps, at DFT B3LYP[GD3BJ]/6-311+G\*\* level.

As aforementioned, the system was studied both in gas and solvated phase. In the latter, three solvents were considered, *viz.* Dimethyl Sulfoxide (DMSO), Ethanol (EtOH), and Water (W). Solvent effects were taken into account in two ways: (1) by means of the implicit Polarizable Continuum Model in its Integral Equation Formalism (IEF-PCM),<sup>15</sup> and (2) by means of different explicit micro-solvation models, wherein one or more molecules of solvents were explicitly placed close to *trans*-CKA<sup>-</sup> and the whole system was treated within IEF-PCM. In the cases of explicit micro-solvation, the number of solvent molecules were 1 (for DMSO, EtOH, and W), 2 (for W) or 3 (for W), placed according to chemical common sense, *i.e.* close to the -NH<sub>2</sub>, >C=O, and -COO<sup>-</sup> groups (see Figure S6). For geometry optimizations and frequency / thermochemical calculations, the PCM molecular cavity was built according to the Universal Force Field (UFF)<sup>16</sup> radii, within the value used in the last implementation of the PCM (based on a continuum surface charge formalism). For the topological analysis and the evaluation of energetics, the Solvation Model based on Density (SMD) parameterization was employed.<sup>17</sup> The standard values for the dielectric constants and refractive indexes were always assumed.

### Electronic excited states

The UV-Vis absorption spectra for the equilibrium geometries were calculated at Time Dependent Density Functional Theory (TD-DFT) level, accounting for  $S_0 \rightarrow S_n$  ( $n = 1$  to 10); the energy of the first 10 triplet states was also computed. The nature of the vertical excited electronic state was analyzed both in gas and solvated phase. This exploration was performed employing the long-range corrected functional CAM-B3LYP<sup>18</sup> coupled with 6-311+G\*\* basis set. The GD3BJ semi-empirical dispersion was also included.

In the case of the solvated phase, the same solvation models as for the ground state were employed. State-specific (SS)<sup>19</sup> treatment of solvent effects was considered, both within the non-equilibrium (neq) and equilibrium (eq) solvation regimes.<sup>20,21</sup> The vibronic progression<sup>22-27</sup> of  $S_0 \rightarrow S_1$  electronic transitions was also simulated, including Duschinsky and Herzberg–Teller effects.

The first singlet  $S(\pi, \pi^*)$  excited state geometry was optimized using analytical gradients and the first transitions  $S_1 \rightarrow S_0$  of the emission transition. Also in this case, SS (both eq and neq) treatment of solvent effects was considered and the electronic emission band was simulated by accounting for the vibronic progressions, as done in the absorption.

The accuracy of the TD-DFT excitation energies and the correctness of the order of the singlet excited states are verified by comparing the TD-DFT results with multi-configurational Complete Active Space Self-Consistent Field (CASSCF)<sup>28</sup> in conjunction with Multi-State Complete Active Space Second Order Perturbation Theory (MSCASPT2)<sup>29</sup> and equation of motion second order coupled cluster (EOM-CC2)<sup>30</sup> results. The full valence  $n-\pi$  active space of *trans*-CKA<sup>-</sup> was considered for CASSCF calculations, without imposing symmetry constraints. In order to incorporate the effect of the dynamic valence electron correlation of the relative energies of the lower ESs, CASPT2 calculations based on the CASSCF reference function were also run. Interaction of CASSCF states via dynamic correlation is taken into account with MS-CASPT2 treatment. CASSCF/CASPT2 calculations were carried out with the 6-311+G\*\* basis set.

Linearly Interpolated Internal Reaction Coordinate (LIIRC) paths were calculated from the Franck-Condon region to the relevant  $S_0/S_1$  conical intersection, to individuate a plausible  $S_1 \rightarrow S_0$  population mechanism. In order to refine the energies of  $S_1$  minima, EOM-CC2 energies were computed at DFT optimized geometries. In PES exploration, CASSCF/CASPT2 methodology was adopted. In these calculations, solvents effects were accounted, by adopting the model of explicit micro-solvation surrounded by a continuum. As solvents, DMSO (one explicit molecule) and W (two explicit molecules) were employed.

#### *Population analyses, topological analyses, and disperse interactions investigation*

The atomic charge population analysis, electric multiple moments, electronic density, and electrostatic potential were also computed within the Mulliken's and CHelpG procedure<sup>31</sup> for both  $S_0$  ground and  $S_1$  excited (vertical and relaxed) states, computed at (TD-)DFT level.

In order to investigate the presence and nature of possible intra-molecular H-bonding interactions, two different approaches were used: on one hand, the topological analysis based on Bader's Atoms in Molecules (AIM) theory,<sup>32,33</sup> and on the other hand, the Non-Covalent Interaction (NCI) Index combined with the second derivative of the Reduced Density Gradient along the second main axis of variation were employed.<sup>34,35</sup> Hessian of electron density was additionally calculated at along RDG isosurface with  $|\text{isovalue}| = 0.5$ .

$$s = \frac{1}{2(3\pi^2)^{1/3}} |\nabla\rho|/\rho^{4/3}, \quad (1)$$

where  $\rho$  is the electron density. These procedures were applied both to the ground and to the first singlet excited (vertical and relaxed) states.

#### *QM/MM calculations*

Experimental spectroscopic data and computed (TD-)DFT findings were set as benchmark data for subsequent steps. Next the photophysical mechanism was simulated in solvated phase. For this aim, a modified variant of the method of Persico *et al.*<sup>36,37</sup> for semiclassical surface-hopping dynamics<sup>38</sup> "on the fly" on non-adiabatically coupled potential energy surfaces is employed. This method involves the following steps: (1) Optimization of the semiempirical parameters. (2) Initialization of a set of trajectories on the ground state by Brownian thermal sampling. (3) Photoexcitation to the target excited electronic state, calculated from a semiempirical configuration interaction (CI) method, by sudden vertical transitions. (4) Propagation of the trajectories on coupled potentials, with gradients and non-adiabatic couplings calculated "on the fly" by the semiempirical CI method and non-adiabatic jumps governed by Tully's surface hopping algorithm.<sup>38</sup> (5) Post-processing calculation of the properties.

The Quantum Mechanical/Molecular Mechanical (QM/MM) system was set up as follows. We distinguished two sub-systems: the solute (CKA<sup>-</sup>) and the solvent. The former was treated at QM level, whereas the latter at MM level. Three solvents were investigated: DMSO, EtOH, and W.

The electronic energies and wave functions of the first five singlet excited states were computed on the fly by a semiempirical Configuration Interaction method based on SCF orbitals with floating occupation numbers (FOMO–CI), suited to represent reactive processes and excited states.<sup>36</sup> The configuration space was a CAS with the whole  $n\pi$  system. All single excitations from seven occupied to six virtual orbitals (in total 94 Slater determinants) were included.

*(1) Optimization of semiempirical parameters.*

As a first step, the semiempirical parameters of the QM sub-system were optimized. The general approach to this problem consist into choose a certain number of properties (geometrical data and energies) in reference to experiments or previously computed (DFT or *ab initio*) data so to find the semiempirical parameters of the different atoms that better which reproduce at QM/MM level the same properties. The initial guess for all the QM atoms (except hydrogen atoms, which were not optimized) in the QM/MM calculations is represented by AM1 semiempirical Hamiltonian. The optimization consists in the minimization of the error function:

$$F = \sqrt{\frac{\sum_i w_i (d_{s,i} - d_{r,i})^2}{\sum_i w_i}}, \quad (2)$$

over all the data computed. In eq. (2)  $d_s$  are the semiempirical results,  $d_r$  the reference data (obtained from experiment and/or high quality calculations) and  $w$  the weights. The data included in the parameter optimization were the initial equilibrium geometry, the  $S_n \leftarrow S_0$  ( $n = 1$  to 5) transition energies, the Potential Energy Surface (PES) ground and  $S_1$  state profile as a function of the torsion around the previously mentioned dihedral angle (the one involved during the photophysical mechanism). During the optimization procedure, the transition energies from  $S_0$  to  $S_n$  were included with different weights ( $w = 1.00$  for  $S_1$  and 0.10 for the others) since in this work the target excited state is  $S_1$ .

*(2) Brownian dynamics.*

This step consists in two sub-steps: (i) Molecular Dynamics (MD) of equilibration of the solvent alone; (ii) QM/MM dynamics of a solute molecule (QM) surrounded by a drop of solvent (MM). The solvents were always represented by the all atom OPLS force-field.<sup>39</sup> The MM description of the solvent and the quantum mechanical (QM) description of CKA<sup>-</sup> (at semiempirical level) are combined in a hybrid QM/MM scheme with electrostatic embedding.<sup>40</sup> The QM/MM interactions are described by Lennard-Jones potentials between the MM and the QM atoms, plus electrostatic interactions that are added to the semiempirical Hamiltonian. The electrostatic potential to which the QM nuclei and electrons are subjected is generated by the MM atomic charges. The latter had the standard OPLS values. The Lennard-Jones parameters have been determined to reproduce the average results obtained at B3LYP[GD3BJ]/6-311+G\*\*//IEF-PCM level on the explicitly micro-solvated CKA<sup>-</sup> with one or more solvent molecules (*vide supra*).

Sub-step (i). We first equilibrated the MM solvent alone, by running 3 ns of  $npT$  MD simulation with periodic boundary conditions. Number of molecules, pressure and temperature were set at 1000, 1.0 atm and 298.15 K, respectively, so to reproduce the experimental densities of the three pure solvents (Table S6). After equilibration, a spherical cluster (drop) of solvent molecules was cut from the cubic cell of the previous simulation final snapshot. All molecules with their centers of

mass within a certain radius  $R_{\text{sph}}$  from the center of the cubic cell were included. The *radii*  $R_{\text{sph}}$  and the numbers of molecules in the drop for each solvent are also shown in Table S6. In order to avoid the loss of molecules by evaporation from the cluster surface, an additional harmonic confining potential was applied to each atom, whose form reads:

$$\Phi(R) \equiv \begin{cases} 0 & \text{for } R \leq R_{\text{wall}} \\ \frac{1}{2}k(R - R_{\text{wall}})^2 & \text{for } R > R_{\text{wall}} \end{cases} \quad (3)$$

wherein  $R$  is the distance of an atom from the center of the sphere,  $k = 0.02$  is an elastic constant, and  $R_{\text{wall}} = R_{\text{sph}} + \delta R$  ( $\delta R = 1 \text{ \AA}$ ).

Table S6. Physical and Geometrical Parameters of the Solvent.

	Dimethyl Sulfoxide (DMSO)	Ethanol (EtOH)	Water (W)
Radius of spherical drop, $R_{\text{sph}}$ ( $\text{\AA}$ )	30	30	32
Number of solvent molecules in the drop	959	1161	4575
- with $\text{CKA}^-$	952	1155	4551
Computed density ( $\text{g/cm}^3$ )	1.100	0.785	0.997
Experimental density <sup>a</sup> ( $\text{g/cm}^3$ )	1.1004	0.78522	0.9970479

<sup>a</sup>  $T = 298.15 \text{ K}$ ,  $p = 1.0 \text{ atm}$ .<sup>41</sup>

Sub-step (ii). In the centre of the solvent drop, a cavity was carved, by taking out a few solvent molecules (see Table S6), so to place the  $\text{CKA}^-$  molecule. For each system, a single Brownian motion trajectory, using (Markovian) Langevin dynamics was run to equilibrate the system. Along this trajectory the system is subject to friction coefficients and random forces. The latter are calculated as Gaussian white noise via the second fluctuation-dissipation theorem from the assumed temperature,  $T$ . The chosen temperatures were always 298.15 K. Equilibration trajectories were run for 100 ps (time step  $\delta t = 0.1 \text{ fs}$ ; the last 50 ps were used to sample the initial conditions for the excited state dynamics), establishing a set of thermal initial conditions for sudden photoexcitation. Along the Brownian trajectory, the electronic spectrum was also simulated.

Each Brownian trajectory was randomly sampled in order to select about 1200 initial conditions for as many Surface Hopping trajectories. The initial conditions were selected according to a Boltzmann distribution in the ground electronic state, weighted with the  $S_1 \leftarrow S_0$  transition probability; at each sampled geometry, a vertical excitation to  $S_1$  was simulated on the basis of its radiative transition probability, actually selecting the sampled set according to a stochastic scheme.<sup>42</sup> In the end, about 1200 sets of initial conditions were selected for each simulation.

(3-4) *Surface Hopping simulations.* Simulations based on Surface Hopping with quantum decoherence corrections<sup>43</sup> of photodynamics were subsequently run, involving the first singlet excited state. The time step  $\delta t = 0.1 \text{ fs}$  for the integration of the trajectories (Beeman-Verlet method) and for the propagation of the electronic wave functions.<sup>36</sup> Ground state plus five electronic excited states ( $S_1$ - $S_5$ ) were included in the dynamics, to allow for possible transitions from  $S_1$  to the upper states. However, very few upward hops were observed. The trajectories were stopped when one of the following conditions was met: (a) the  $\text{CKA}^-$  molecule has reached its electronic ground state; (b) the total time reached 20 ps; or, (c) the total time exceeded 2 ps, the system reverted back to the ground state and reached a the geometry corresponding to the conical intersection (*vide supra*).



Data were finally post-processed, so to evaluate average geometrical and spectroscopical (UV-Vis spectra) properties of solvated  $\text{CKA}^-$  and the population's decay as a function of time (with subsequent evaluation of characteristic times and fluorescence quantum yield).

#### *Other technical details and used codes*

Concerning (TD-)DFT calculations, integration grid for the electronic density for topological and RDG analyses was set to 150 radial shells and 974 angular points. For rest calculations integration grid set as 99 radial shells and 590 angular points. Convergence criteria of Self-Consistent Field was set to  $10^{-12}$  for RMS change in density matrix and  $10^{-10}$  for maximum change in density matrix. Convergence criteria for optimizations were set to  $2 \times 10^{-6}$  a.u. for maximum force,  $1 \times 10^{-6}$  a.u. for RMS force,  $6 \times 10^{-6}$  a.u. for maximum displacement and  $4 \times 10^{-6}$  a.u. for RMS displacement.

All CASPT2 calculations have been performed using an imaginary level shift of 0.20 a.u., in order to avoid the incorporation of intruder states, and a standard value for IPEA shift of 0.25 a.u.

(TD-)DFT calculations were performed using GAUSSIAN G09.D01 package.<sup>44</sup> Location of BCPs and subsequent calculation of SF values were performed using a modified version of the PROAIMV program.<sup>45-47</sup> The calculation of the RDG and its derivatives were performed using homemade codes. CASSCF and CC2 calculations were performed using MOLCAS<sup>48</sup> and DALTON<sup>49</sup> codes. QM/MM calculations were performed with a development version of the MOPAC<sup>50</sup> semiempirical code linked with the molecular mechanics package TINKER.<sup>51</sup> The MOSCITO package was employed in equilibration MD simulations for pure solvents.<sup>52</sup>

## References

1. Calvert, J.R.; Pitts, J. N. Photochemistry. John Willey, Springer, 1969.
2. Morandeira, A.; Engeli, L; Vauthey, E. Ultrafast Charge Recombination of Photogenerated Ion Pairs to an Electronic Excited State. *J Phys Chem A*. **2002**, *106*, 4833–4837.
3. Duvanel, G.; Grilj, J.; Chaumeil, H.; Jacques, P.; Vauthey, E. Ultrafast excited-state dynamics of a series of zwitterionic pyridinium phenoxides with increasing sterical hindering. *Photochem. Photobiol. Sci.* **2010**, *9*, 908–915.
4. Duvanel, G.; Banerji, N.; Vauthey, E. Excited-state dynamics of donoracceptor bridged systems containing a boron-dipyrromethene chromophore: interplay between charge separation and reorientational motion. *J. Phys. Chem. A* **2007**, *111*, 5361–5369.
5. Banerji, N.; Duvanel, G.; Perez-Velasco, A.; Maity, S.; Sakai, N.; Matile, S.; Vauthey, E. Excited-state dynamics of hybrid multichromophoric systems: toward an excitation wavelength control of the charge separation pathways. *J. Phys. Chem. A.*, **2009**, *113*, 8202.
6. Tsentalovich, Y. P.; Sherin, P. S.; Kopylova, L. V.; Cherepanov, I. V.; Grilj, J.; Vauthey, E. Photochemical properties of UV filter molecules of the human eye. *Invest. Ophthalmol. Vis. Sci.* **2001**, *52*, 7687–7696.
7. Sherin, P. S.; Zelentsova, E. A.; Sormacheva, E. D.; Yanshole, V. V.; Duzhak, T. G.; Tsentalovich, Yu. P. Aggregation of  $\alpha$ -crystallins in kynurenic acid-sensitized UVA photolysis under anaerobic conditions. *Phys. Chem. Chem. Phys.* **2016**, *18*, 8827–8839.
8. Becke, A. D. Density-Functional Thermochemistry. III. The Role of Exact Exchange. *J. Chem. Phys.* **1993**, *98* (7), 5648–5652.

9. Zhao, Y.; Truhlar, D. G. The M06 Suite of Density Functionals for Main Group Thermochemistry, Thermochemical Kinetics, Noncovalent Interactions, Excited States, and Transition Elements: Two New Functionals and Systematic Testing of Four M06-Class Functionals and 12 Other Function. *Theor. Chem. Acc.* **2008**, *120* (1–3), 215–241.
10. Chai, J. Da; Head-Gordon, M. Systematic Optimization of Long-Range Corrected Hybrid Density Functionals. *J. Chem. Phys.* **2008**, *128* (8), 84106.
11. Ditchfield, R. Self-Consistent Molecular-Orbital Methods. IX. An Extended Gaussian-Type Basis for Molecular-Orbital Studies of Organic Molecules. *J. Chem. Phys.* **1971**, *54* (2), 724–728.
12. McLean, A. D.; Chandler, G. S. Contracted Gaussian-Basis Sets for Molecular Calculations. 1. 2nd Row Atoms, Z=11-18. *J. Chem. Phys.* **1980**, *72*, 5639–5648.
13. Krishnan, R.; Binkley, J. S.; Seeger, R.; Pople, J. A. Self-Consistent Molecular Orbital Methods. XX. A Basis Set for Correlated Wave Functions. *J. Chem. Phys.* **1980**, *72* (1), 650–654.
14. Grimme, S.; Ehrlich, S.; Goerigk, L. Effect of the Damping Function in Dispersion Corrected Density Functional Theory. *J. Comput. Chem.* **2011**, *32*, 1456–1465.
15. Tomasi, J.; Mennucci, B.; Cancès, E. The IEF version of the PCM solvation method: an overview of a new method addressed to study molecular solutes at the QM *ab initio* level. *J. Mol. Struct.: Theochem* **1999**, *464*, 211-226.
16. Rappé, A.K.; Casewit, C.J.; Colwell, K.S.; Goddard, W.A.; Skiff, W.M. UFF, a full periodic table force field for molecular mechanics and molecular dynamics simulations. *J. Am. Chem. Soc.* **1992**, *114*, 10024-10035.
17. Marenich, A. V.; Cramer, C. J.; Truhlar, D. G. Universal solvation model based on solute electron density and a continuum model of the solvent defined by the bulk dielectric constant and atomic surface tensions, *J. Phys. Chem. B* **2009**, *113*, 6378-6396.
18. Yanai, T.; Tew, D. P.; Handy, N. C. A New Hybrid Exchange-Correlation Functional Using the Coulomb-Attenuating Method (CAM-B3LYP). *Chem. Phys. Lett.* **2004**, *393* (1–3), 51–57.
19. Impropa, R.; Barone, V.; Scalmani, G.; Frisch, M. J. *J. Chem. Phys.* **2006**, *125*, 054103-1-054103-9.
20. Barone, V. *Computational Strategies for Spectroscopy: From Small Molecules to NanoSystems*; Wiley-WCH: Chichester, UK, **2011**.
21. Mennucci, B.; Cappelli, C.; Guido, C. A.; Cammi, R.; Tomasi, J. *J. Phys. Chem. A* **2009**, *113*, 3009-3020.
22. Santoro, F.; Impropa, R.; Lami, A.; Bloino J.; Barone, V. *J. Chem. Phys.* **2007**, *126*, 169903.
23. Santoro, F.; Lami, A.; Impropa, R.; Barone, V. *J. Chem. Phys.* **2007**, *126*, 184102:1-11.
24. Santoro, F.; Impropa, R.; Lami, A.; Bloino, J.; Barone, V. *J. Chem. Phys.* **2008**, *128*, 224311:1-17.
25. Dierksen M.; Grimme, S. *J. Chem. Phys.* **2005**, *122*, 244101:1-4.
26. Jankowiak, H.-C.; Stuber, J. L.; Berger, R. *J. Chem. Phys.* **2007**, *127*, 234101:1-23.
27. Borrelli, R.; Capobianco, A.; Peluso, A. *Can. J. Chem.* **2013**, *91*, 495-504.
28. Roos, B. O.; Taylor, P. R.; Sigbahn, P. E. *Chem. Phys.* **1980**, *48*, 157-173.
29. Finley, J.; Malmqvist, P.; Roos, B. O.; Serrano-Andrés, L. *Chem. Phys. Lett.* **1998**, *288*, 299-306.
30. Krylov, A. I. *Ann. Rev. Phys. Chem.* **2008**, *59*, 433-462.
31. Breneman, C. M.; Wiberg, K. B. *J. Comp. Chem.* **1990**, *11*, 361-373.
32. Bader, R. F. W.; Essen, H. J. *J. Chem. Phys.* **1984**, *80*, 1943-1960.

33. Bader, R. F. W. *Atoms in molecules. A quantum theory*; Oxford University Press: Oxford, **1990**.
34. Bohórquez, H. J.; Matta, C. F.; Boyd, R. J. *Int. J. Quant. Chem.* **2010**, *110*, 2418-2425.
35. Johnson, E. R.; Keinan, S.; Mori-Sanchez, P.; Contreras-Garcia, J.; Cohen, A. J.; Yang, W. *J. Am. Chem. Soc.* **2010**, *132*, 6498-6506.
36. Granucci, G.; Persico, M.; Toniolo, A. *Direct semiclassical simulation of photochemical processes with semiempirical wave functions. J. Chem. Phys.* **2001**, *114*, 10608.
37. Ciminelli, C.; Granucci, G.; Persico, M. *The Photoisomerization Mechanism of Azobenzene: A Semiclassical Simulation of Nonadiabatic Dynamics. Chem.–Eur. J.* **2004**, *10*, 2327-2341.
38. Tully, J. C. *Molecular dynamics with electronic transitions. J. Chem. Phys.* **1990**, *93*, 1061.
39. Jorgensen, W. L.; Tirado-Rives, J. *J. Am. Chem. Soc.* **1988**, *110*, 1657.
40. Persico, M.; Granucci, G.; Inglese, S.; Laino, T.; Toniolo, A. *J. Mol. Struct. THEOCHEM* **2003**, *621*, 119.
41. Lide, D. R. *CRC Handbook of Chemistry and Physics* (97th ed.). Boca Raton, Florida: CRC Press, **2016**.
42. Creatini, L.; Cusati, T.; Granucci, G.; Persico, M. Photodynamics of azobenzene in a hindering environment. *Chem. Phys.* **2007**, *347*, 492–502.
43. Granucci, G.; Persico, M. Critical appraisal of the fewest switches algorithm for surface hopping. *J. Chem. Phys.* **2007**, *126*, 134114.
44. Frisch, M. J.; Trucks, G. W.; Schlegel, H. B.; Scuseria, G. E.; Robb, M. A.; Cheeseman, J. R.; Scalmani, G.; Barone, V.; Mennucci, B.; Petersson, G. A.; Nakatsuji, H.; Caricato, M.; Li, X.; Hratchian, H. P.; Izmaylov, A. F.; Bloino, J.; Zheng, G.; Sonnenb, D. J. *et al.* Gaussian 09, Revision D.01. *Gaussian, Inc., Wallingford CT* **2009**.
45. Biegler-König, F. W.; Bader, R. F. W.; Tang, T. H. *J. Comput. Chem.* **1982**, *3*, 317-328.
46. AIMPAC, [www.chemistry.mcmaster.ca/aimpac/imagemap/imagemap.htm](http://www.chemistry.mcmaster.ca/aimpac/imagemap/imagemap.htm)
47. Keith, T. *Ph.D. Thesis*, Ontario, Canada, **1993**.
48. Aquilante, F.; De Vico, L.; Ferré, N.; Ghigo, G.; Malmqvist, P.; Neogrády, P.; Pedersen, T. B.; Pitonák, M.; Reiher, M.; Roos, B. O.; Serrano-Andrés, L.; Urban, M.; Veryazov, V.; Lindh, R. *J. Comp. Chem.* **2010**, *31*, 224-247.
49. Aidas, K.; Angeli, C.; Bak, K. L.; Bakken, V.; Bast, R.; Boman, L.; Christiansen, O.; Cimiraglia, R.; Coriani, S.; Dahle, P.; Dalskov, E. K.; Ekström, U.; Enevoldsen, T.; Eriksen, J. J.; Ettenhuber, P. *et al.* *Wiley Interdisciplinary Reviews: Computational Molecular Science* **2014**, *4*, 269-284.
50. Stewart, J. J. P. *MOPAC*; Fujitsu Limited, Tokyo, Japan, **2002**.
51. Ponder, J. W. *TINKER 6.1*; Washington University School of Medicine: St. Louis, MO: **2012**. <http://dasher.wustl.edu/tinker>.
52. Paschek, D.; Geiger, A. *MOSCITO 3.9*; Department of Physical Chemistry, University of Dortmund: **2000**.